Mechanosensitive single molecule dynamics of myosin II

Author: Mariona Colomer Rosell
Facultat de Física, Universitat de Barcelona, Diagonal 645, 08028 Barcelona, Spain
Institut de Ciències Fotòniques, The Barcelona Institute of Science and Technology, 10 08860 Castelldefels, Spain

Advisors: Valeria Venturini and Stefan Wieser
UB Advisor: Jaume Casademunt

Abstract: In this project we have characterised the dynamics of single myosin II molecules in stem cells under mechanical stress combining high spatial and time resolution microscopy with image analysis and simulations. We show that in the bleb, intensity of myosin spots increases as they assemble into bipolar thick filaments. In comparison with the myosin II under the nucleus, in the bleb they undergo a super diffusive motion which could drive the bleb contraction. We have analysed their spatial distribution using DBSCAN clustering analysis and we have performed Cytosim simulations to study the myosin II dynamics in the retraction bleb. This analysis sets the framework and the computational pipeline for further experiments.

I. INTRODUCTION

Cells experience different microenvironments depending, for example, on the tissues and developmental stages they are and these include both biochemical signalling and physical changes such as mechanical forces. These forces lead to shape changes but could also induce a variety of active responses like cell polarization and migration. Our last work showed that forces can be quantitatively measured and characterised at the single cell level thanks to the mechanosensitive properties of the nucleus and that cells respond to them by regulating myosin II activity[1] [2].

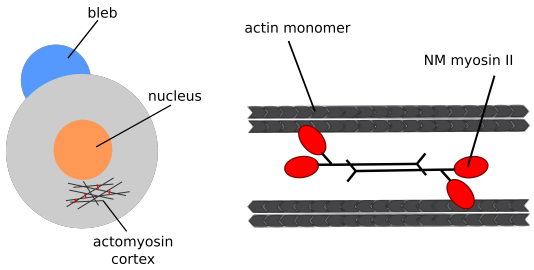

FIG. 1: Sketch of the acto-myosin cell cortex. It is formed by actin filaments and NM myosin II motors.

The cellular skeleton, or actomyosin cortex, is composed of two main molecules; actin and myosin as shown in Figure 1. This structure gives rigidity to the cell but it is also highly dynamic and its spatiotemporal regulation allows for shape changes and active force generation for example. Most of these processes involve a differential regulation of actin and myosin and their interplay, which can lead to differences on cell contractility [3] [4]. When cells are highly contractile, their intracellular pressure is high and this leads to the formation of blebs which are membrane based cellular protrusion. Both actin and myosin diffuse into the newly formed bleb until forming a stable cortex that can retract [5].

Actin monomers polymerize into filaments while nonmuscle myosin II (NMII) are motor proteins that can bind to these filaments. NMII are polar monomers formed of two heavy chains, two regulatory chains and two light chains and can be activated [6] [7]. Myosin monomers assemble into antiparallel structures called bipolar thick filaments (BTFs) (Figure 2). The BTFs are the functional unit, able to exert forces to actin filaments by activating myosin II. This simple interaction controls active shape change, cell polarisation and migration [8].

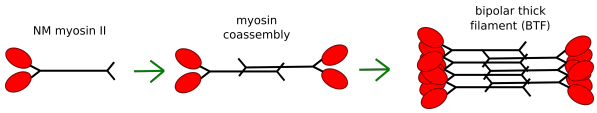

FIG. 2: Non muscle myosin II co-assemble forming bipolar thick filaments.

The separation between the two poles of the bipolar filaments is around 300 nm which is of the order of the wavelength of visible light [9]. Conventional microscopy is diffraction-limited which restricts the resolution that we can achieve. However, the development of state-of-the art micorscopy techniques such as TIRF microscopy [10] and super-resolution microscopes now allow us the imaging of these molecules in a living cell by surpassing the spatial resolution (SIM) or increasing the signal-to-noise ratio (SNR) of the molecules at the surface of the cell (TIRF) [11] [12].

In this project, we will use a TIRF microscope. In this technique, the sample is illuminated at the critical angle: the excitation light undergoes total internal reflection and the fluorophores are excited with an evanescent wave whose intensity decreases exponentially from the glass. This increases the SNR ratio and reduces the photobleaching in the whole cell [10].

Although some studies have been carried out in myosin dynamics in vitro [13] and some simulations [14], still little is known about how myosin molecules coassemble and move in a living cell. In this study we are going to characterise the dynamics and clustering of single myosin molecules upon stress combining high spatial and time resolution microscopy with image analysis and simulations.

II. EXPERIMENTAL PROCEDURE AND ANALYSIS

A. Experimental setup and procedure

Images were acquired using a custom-built TIRF microscope with an Andor Zyla 4.2 (sCMOS) camera, two-colour lasers 473GEM and 561GEM by LaserQuantum and a UPLAPO100XOHR objective by Olympus. The laser 473GEM excites the green fluorescent protein GFP (488 nm). A transgenic zebrafish line with eGFP fused to MyI12.1 (so, MyI12.1-eGFP) was used in order to obtain progenitor stem cells. Single cells were dissociated from embryos at 4 hours post fertilization. Confinement size was controlled using a dynamic micro-confiner and cells were confined at a height of 7 μm to introduce a mechanical stress. Temperature was set at T=28.5 ^{o}C using a temperature controller. The frame rate used was 500 ms and videos were recorded for $>$ 60 s (Figure 3).

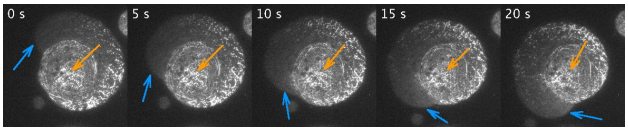

FIG. 3: TIRF time lapse a of a MyI12.1-eGFP stem cell blebbing under confinement. Arrows show the bleb (blue) and the nucleus region (orange).

B. Image analysis

Image files were processed using Fiji [15]. Each single molecule was tracked using the Trackmate plugin [16] and a custom-written Macro for Fiji. The background intensity (I_{bkgd}) of the cytosol was also tracked over time and averaged. The normalised intensity over time was $I(t) = \frac{I - I_{bkgd}}{I_{max} - I_{bkgd}}$.

The mean squared displacement (MSD) as a function of the time lag can be used to determine the type of diffusion that myosins undergo. MSD is computed as:

$$MSD(\tau) = \langle [\vec{r}(t+\tau) - \vec{r}(t)]^2 \rangle \tag{1}$$

It can be fitted to an exponential function to determine the diffusion mode:

$$MSD(\tau) = 2nD\tau^{\alpha} \begin{cases} \text{superdiffusion} & \text{if } 1 < \alpha < 2 \\ \text{normal diffusion} & \text{if } \alpha \approx 1 \\ \text{subdiffusion} & \text{if } \alpha < 1 \end{cases}$$

where D is the diffusion constant and n the dimension which in this case will be $n = 2$.

Once the bleb starts forming, its myosin density increases and we can see that myosins form clusters. We can analyse the clustering of myosin molecules using the DBSCAN method which is a data clustering algorithm. This method is very efficient to find clusters of arbitrary sizes and shapes and it only requires two parameters: ϵ which is the maximum distance between two myosins from the same cluster and $minPts$ which is the minimum number of myosins that forms a cluster.

C. Cytosim simulations

To have a better understanding of the myosin diffusion in the cell, simulations have been performed with Cytosim [17] [18]. The modelled actomyosin network consists on flexible actin filaments, active myosin motors and crosslinkers connectors. Firstly, all the fibers and connectors are described by points. Their coordinates are collected in a vector $\vec{x}$ and follow the Langevin equation of motion:

$$d\vec{x} = \mu F(\vec{x}, t)dt + dB(t) \tag{2}$$

where basically $F(\vec{x}, t)$ are the forces that act on the point at the concerned time, μ is a matrix with the mobility coefficients of each point and $dB(t)$ is an stochastic term that follows the Brownian motion [19].

Actin filaments are simulated as 2 μm flexible fibers made from small segments and a rigidity of 75 pN/μm^2. They are modelled as a linear set of points which can experiment contraction, bending and expansion depending on their elasticity.

Connectors such as myosin motors or crosslinkers are modelled as Hookean springs that bind between actin filaments (points a and b) with a constant spring $k_{stiffness}$ and a r resting length:

$$f = k_{stiffness}\left(1 - \frac{r}{|\delta|}\right)\delta \tag{3}$$

where $\delta = a - b$. Myosins are active connectors simulated by two hand motors that bind to the filament and move towards the end of it. In the simulation, myosins have a binding rate of $k_{on} = 10$ s^{-1} and a binding range

of 0.01 μm. They can also unbound from the actin filaments with a $k_{off} = 0.5$ s^{-1}. Their dwell movement is described as:

$$v = v_m \left(1 - \frac{f}{f_s}\right) \tag{4}$$

Where $v_m = 2$ μm/s and the stall force is $4pN$. However, myosin alone can not produce contraction since their dwelling at the end of the filaments produces the so-called filament sliding. To simulate contractility, we need crosslinkers which are passive connectors. Crosslinkers bind to the filaments and remain immobile in their positions until they detach. Their binding rates and ranges are set as $k_{on} = 10$ s^{-1}, $k_{off} = 0.5$ s^{-1} and $range = 0.01$ μm [20]. Contractility can be estimated by computing the effective radius of the cell:

$$R = \sqrt{\frac{2}{P}\sum_i r_i^2} \tag{5}$$

Then, contraction rate is defined as $dR/dt = [R(t + \Delta t) - R(t)]/\Delta t$ [20]. At the page `github.com/mcolomerr/TFG` you can find all the scripts written for the analysis and the simulations.

III. RESULTS

A. Dynamics of the NMII and BTF growth

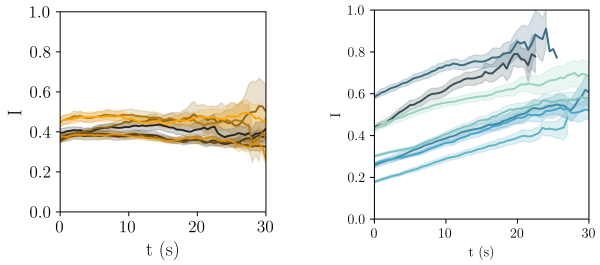

FIG. 4: Normalised intensity over time of myosins at the bleb and at the nucleus for $n_{cells} = 7$ and $n_{tracks} > 50$ each cell. Confidence intervals estimated with the standard deviation of the data.

Tracking of single myosins reveals differences between the normalised intensity in the bleb region and under the nucleus as Figure 4 shows. In the bleb, the particle intensity increase over time while the intensity of the particles under the nucleus remains constant. Therefore, we can see the global accummulation of myosins and the formation of the BTFs in the bleb.

The MSD as a function of time lag curves show differences on the dynamics of NMII in the bleb formation and under the nucleus as Figure 5 illustrates. These differences can be further studied by fitting an exponential function $MSD(\tau) = 4D\tau^{\alpha}$.

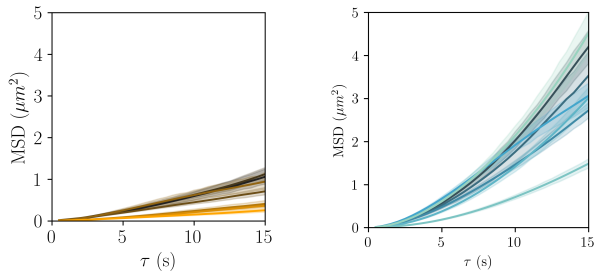

FIG. 5: Mean squared displacement (MSD) curves as a function of time lag of the myosin tracks at the bleb and at the nucleus for $n_{cells} = 7$ and $n_{tracks} > 50$ each cell. Confidence intervals estimated with the standard deviation of the data.

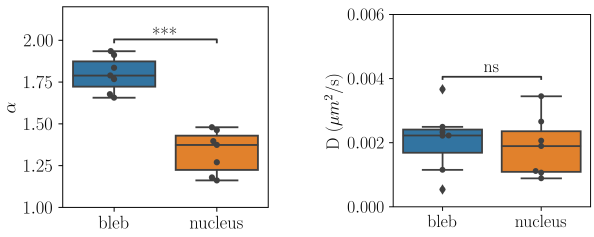

FIG. 6: α and D coefficients of the myosin tracks at the bleb and under the nucleus obtained fitting the equation $MSD(\tau) = 4D\tau^{\alpha}$. Significance bars computed with the paired t-test: *** $p < 0.001$, ns (non significant) $p > 0.05$.

Interestingly, in Figure 6 we can see that in both regions the myosins have a similar diffusion constant and that their movement is characterised by the parameter α with significant differences. In the bleb, myosins experiment a super-diffusion movement characterised with an $\alpha = 1.80 \pm 0.14$ which could drive the contraction rate of the cell. Whereas under the nucleus, the diffusion movement is described by an $\alpha = 1.39 \pm 0.10$ closer to a pure diffusion movement. There are no significant differences in the parameter D.

B. Analysis of the spatial distribution of the myosin filaments

Apart from the described growth of the BTF, there is also an increase in the number of myosin spots in the bleb, while in the nucleus it remains constant (Figure 7).

Using the DBSCAN clustering algorithm, we found out

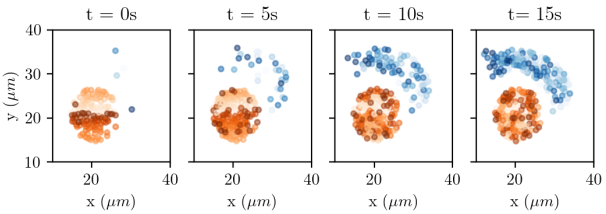

FIG. 7: Evolution of the number of spots over time in the nucleus (orange) and in the bleb (blue).

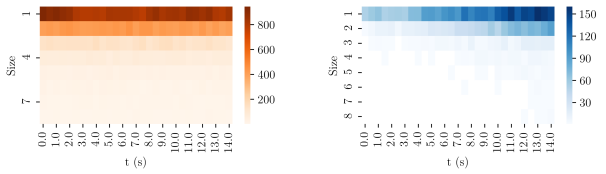

Nucleus Bleb

FIG. 8: Diagram with the number of clusters and cluster sizes over time with an $\epsilon = 400$ nm.

that in the bleb both the size and number of clusters increases over time while in the nucleus it remains constant as Figure 8 illustrates. The growth of the clusters shows that the NMII creates a network and the binding of myosin molecules at the actin filaments could enhance the binding of more molecules nearby. This part can be further studied using two-colour experiments of actin and myosin.

C. Simulation of the spatial distribution and dynamics of NMII

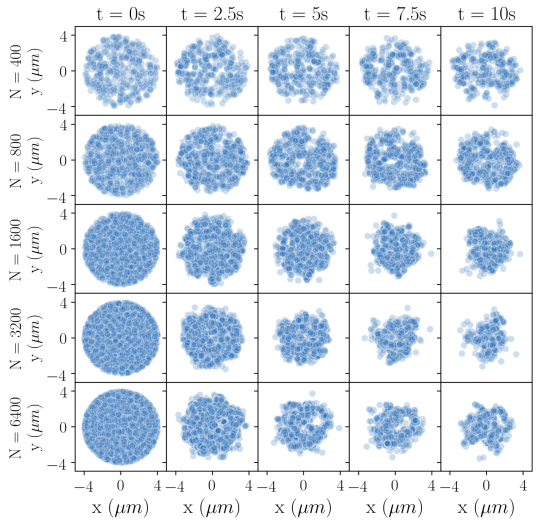

FIG. 9: Distribution of myosins in a simulated cell over time for different myosin concentrations, 400 actin filaments and 3200 crosslinkers.

Simulating the actomyosin network using Cytosim [17], we see that different ratios of myosin-actin lead to different contraction rates as Figure 9 illustrates. Thus, the different behaviour of NMII at the bleb and at the nucleus could be explained by the relative concentration of myosins in these two regions produced by the activation of NMII through the mechanosensation process.

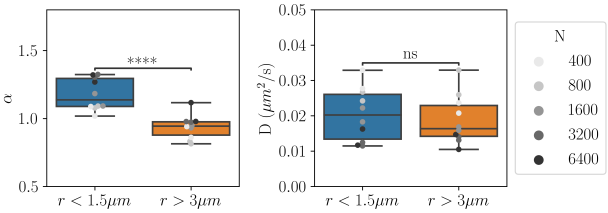

FIG. 10: α and D coefficients of the simulated myosin tracks at different R_{max} obtained fitting the equation $MSD(\tau) = 4D\tau^{\alpha}$. Significance bars computed with the paired t-test: **** $p < 10^{-4}$, ns (non significant) $p > 0.05$.

Analysis of the MSD curves show that the α parameter depends significantly on the position of the track (Figure 10). For tracks with $R_{max} > 3$ μm, the α are in the superdiffusive range while for tracks with $R_{max} < 1.5$ μm the α are in the diffusive range. Thus, as in our experimental data, NMII tracks are more directional in the bleb than in the center of the cell and we can hypothesise that myosin II at the bleb could drive the bleb retraction.

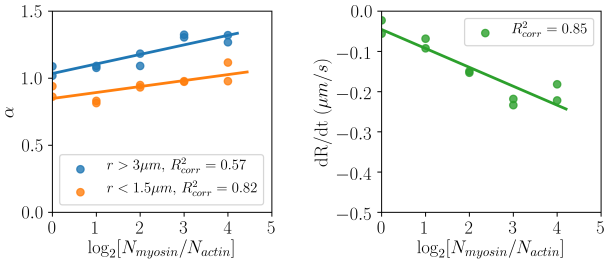

FIG. 11: α coefficients of the simulated myosin tracks at different R_{max} and contraction rate as a function of the relative concentration of myosins to actin filaments ($N = 400$). $R^2{}_{corr}$ is the squared correlation coefficient.

The relative concentration of myosin to actin also seems to play a role in the increase of contractility. α coefficients of the NMII tracks increase with the myosin-actin ratio both at the center and at the edge of the cell. Therefore, a high ratio of N_{myosin}/N_{actin} could explain the retraction of the bleb and the different NMII diffusion behaviours. If we study how the effective radius changes over time, we see that the negative expansion rate decreases with the myosin relative concentration as in Figure 11. We see that these rates are similar to the speeds of the tracks at the bleb. Therefore, the NMII tracks at the bleb could be driven by the bleb retraction.

IV. CONCLUSIONS

- TIRF microscopy allowed us to observe that NMII molecules increase in intensity and number during bleb growth in stem cells under mechanical confinement. The increase on intensity shows the coassembly of NM myosin II into BTF.
- Differences between the dynamics of NMII in the bleb and under the nucleus show that in the bleb NMII are super-diffusive whereas in the nucleus they are more diffusive.
- DBSCAN cluster analysis reveals that both the number of NMII clusters and their size increase when the bleb is growing. This could be due to a positive-feedback of NMII binding to actin and it will be further studied with two-colour experiments of actin and myosin.
- Cytosim simulations show that a relatively high concentration of myosin results in an increase of the α coefficient and the contraction rate. Thus, a high ratio of myosin molecules to actin filaments and the superdiffusion movement of NMII in the bleb could drive the contraction of the cell.
- This work has set the framework and the data analysis pipeline to optimise further experiments which will study how NMII behaves under different mechanical conditions.

Acknowledgments

I wholeheartedly would like to thank Valeria Venturini for her guidance and help. I would also like to thank Dr. Stefan Wieser and Dr. Verena Ruprecht for their supervision and Prof. Jaume Casademunt for being my UB advisor. Finally, I wish to express my gratitude to my sister, my mum and my dad for all their support. This work has been supported by an ICFO Maria Yzuel Fellowship Award.

[1] Valeria Venturini et al. "The nucleus measures shape deformation for cellular proprioception and regulates adaptive morphodynamics". In: *bioRxiv* (2019). DOI: 10.1101/865949. URL: https://www.biorxiv.org/content/early/2019/12/05/865949.

[2] Alexis Lomakin et al. "The nucleus acts as a ruler tailoring cell responses to spatial constraints". In: *bioRxiv* (2019), p. 863514.

[3] Tatyana M Svitkina. "Ultrastructure of the actin cytoskeleton". In: *Current opinion in cell biology* 54 (2018), pp. 1–8.

[4] Gijsje H Koenderink and Ewa K Paluch. "Architecture shapes contractility in actomyosin networks". In: *Current opinion in cell biology* 50 (2018), pp. 79–85.

[5] Guillaume T Charras et al. "Non-equilibration of hydrostatic pressure in blebbing cells". In: *Nature* 435.7040 (2005), pp. 365–369.

[6] Mira Krendel and Mark S Mooseker. "Myosins: tails (and heads) of functional diversity". In: *Physiology* 20.4 (2005), pp. 239–251.

[7] B. Alberts. *Molecular Biology of the Cell*. CRC Press, 2017. ISBN: 9781317563754. URL: https://books.google.es/books?id=jK6UBQAAQBAJ.

[8] Miguel Vicente-Manzanares et al. "Non-muscle myosin II takes centre stage in cell adhesion and migration". In: *Nature reviews Molecular cell biology* 10.11 (2009), pp. 778–790.

[9] Jordan R Beach et al. "Nonmuscle myosin II isoforms coassemble in living cells". In: *Current Biology* 24.10 (2014), pp. 1160–1166.

[10] Daniel Axelrod. "Total internal reflection fluorescence microscopy in cell biology". In: *Traffic* 2.11 (2001), pp. 764–774.

[11] Eric Betzig et al. "Imaging intracellular fluorescent proteins at nanometer resolution". In: *Science* 313.5793 (2006), pp. 1642–1645.

[12] Zhe Liu, Luke D Lavis, and Eric Betzig. "Imaging live-cell dynamics and structure at the single-molecule level". In: *Molecular cell* 58.4 (2015), pp. 644–659.

[13] Lewis S Mosby et al. "Myosin II filament dynamics in actin networks revealed with interferometric scattering microscopy". In: *Biophysical Journal* (2020).

[14] Atsushi Matsuda et al. "Mobility of Molecular Motors Regulates Contractile Behaviors of Actin Networks". In: *Biophysical journal* 116.11 (2019), pp. 2161–2171.

[15] Johannes Schindelin et al. "Fiji: an open-source platform for biological-image analysis". In: *Nature methods* 9.7 (2012), pp. 676–682.

[16] Jean-Yves Tinevez et al. "TrackMate: An open and extensible platform for single-particle tracking". In: *Methods* 115 (2017), pp. 80–90.

[17] Julio M Belmonte, Maria Leptin, and François Nédélec. "A theory that predicts behaviors of disordered cytoskeletal networks". In: *Molecular Systems Biology* 13.9 (2017).

[18] Daniel B Cortes et al. "Bond type and discretization of non-muscle myosin II are critical for simulated contractile dynamics". In: *Biophysical Journal* (2020).

[19] Francois Nedelec and Dietrich Foethke. "Collective Langevin dynamics of flexible cytoskeletal fibers". In: *New Journal of Physics* 9.11 (2007), p. 427.

[20] Viktoria Wollrab et al. "Polarity sorting drives remodeling of actin-myosin networks". In: *J Cell Sci* 132.4 (2019), jcs219717.